PACS numbers: 52.38.Mf; 61.43.Hv
DOI: 10.1070/QE2002v032n05ABEH002214

Efficiency of fractal structure formation during laser evaporation

N.E. Kask, E.G. Leksina, S.V. Michurin, G.M. Fedorov, D.B. Chopornyak

***Abstract*. The formation of fractals during laser evaporation of various media (metals and dielectrics) by 10-ms Nd laser pulses is studied experimentally as a function of the laser radiation power density and external pressure. It is established that fractals are formed during the action of a laser pulse in the bulk of a plasma plume. It is found that finely dispersed phase forms under a certain critical pressure a bound shell (macrofractal) in peripheral layers of the plume. The presence of the shell confining the plasma expansion leads to a threshold variation of the characteristics of the optical discharge.**

Keywords: *optical discharge, fractal structures, plasma, percolation.*

1. Introduction

Laser-induced evaporation of substances (including refractory materials) provides the highly efficient production of compact clusters and their aggregates. First, molecular associates (dimers, trimers, etc.), whose concentration may reach 10 % of the monomer concentration, are formed in saturated vapour [1]. Approximately 10^{-4} s later, compact clusters containing $10^3 - 10^4$ atoms appear due to vapour condensation and coagulation of nuclei in cooled liquid layers of the vapour – gas flow [2].

The efficiency of clusterisation increases in the atmosphere of a buffer gas absorbing the excess energy released during condensation. Compact clusters with the characteristic size ~ 10 nm aggregate to form fractal clusters (aggregates) of size ~ 1 μm. Such clusters are observed $\sim 10^{-2}$ s after the action of a millisecond laser pulse with a power density of $10^6 - 10^7$ W cm^{-2} [3]. In an external electric field, fractal aggregates are assembled into filamentary macrostructures.

In experiments described in Ref. [3], fractal filaments appear $10^2 - 10^3$ s after the action of a laser pulse. A mechanism of macrostructure formation other than aggregation is obviously realised in the case of a longer action of a laser pulse and, accordingly, at a higher concentration of finely dispersed fraction in the bulk of the plume. For example, an order-of-magnitude increase in the laser pulse duration results in the formation of macrostructures after $\sim 10^{-2}$ s even in the absence of an external field [4, 5]. It is assumed that the mechanism of macrostructure formation is triggered in this case by a percolation transition in an aggregate of microfractals. When the concentration of isolated fractal aggregates increases during evaporation and achieves its critical value, the aggregates are combined to form a bound macroscopic fractal structure.

Note that the dependences of the optical and electrical properties of a laser plasma on its composition, which are typical of percolation, were also observed during laser-induced evaporation of binary targets [6]. Fractal structures are formed from solid particles; in the case of laser-induced evaporation, they are formed in peripheral layers of the plume, which are cooled to a temperature below the melting point. Cold layers containing fractals may not only distort the optical and electrical characteristics of the discharge region, but also considerably affect the state and dynamics of the plasma, confining its expansion.

An increase in the density of the disperse phase in a gas-discharge plasma leads to a transition to condensed phases ('liquid plasma' and 'plasma crystal') in which ordered bound structures coexist with individual plasma components (electrons, ions and microclusters). It is known [7] that bound dust agglomerates are formed when the microcluster concentration exceeds a certain threshold value, which is also typical of percolation. A transition to the condensed state occurs irrespective of the shape of the charged dust particles (compact or fractal microclusters [8]), and is accompanied by a sharp change in the plasma emission.

Experiments with an optical-discharge plasma initiated and sustained by laser radiation at the surface of a condensed matter makes it possible to vary the media and external parameters under study in broad ranges, leading to a change in the size of clusters and their dimensionality. In order to determine the role of percolation and aggregation in the plasma plume, it would be interesting to analyse the efficiency of the process of fractal formation as a function of external conditions (buffer gas pressure, experimental geometry, laser radiation power density, etc.). The experimental dependences presented below allow us to analyse the correlation in the percolation and the processes of fractal formation and condensation in a plasma with finely dispersed phase.

N.E. Kask, E.G. Leksina, S.V. Michurin, G.M. Fedorov, D.B. Chopornyak
D.V. Skobel'tsyn Research Institute for Nuclear Physics, Moscow State University, Vorob'evy gory, 119992 Moscow, Russia;
e-mail: nek@srdlan.sinp.msu.ru

Received 4 February 2002
Kvantovaya Elektronika **32** (5) 437 – 442 (2002)
Translated by Ram Wadhwa

2. Experimental

The scheme of the experimental setup is shown in Fig. 1. In order to obtain the pressure dependences, the target under study was placed in a sealed chamber (the diameter and length of the inner cavity were 25 and 150 mm, respectively). The pressure of the inert buffer gas (Ar, He) could be varied from 0.001 to 100 atm. The target was evaporated under the action of a quasi-continuous bell-shaped laser pulse with the FWHM of about 10 ms. The energy of the incident beam was varied by means of neutral light filters in the range from 10 to 200 J.

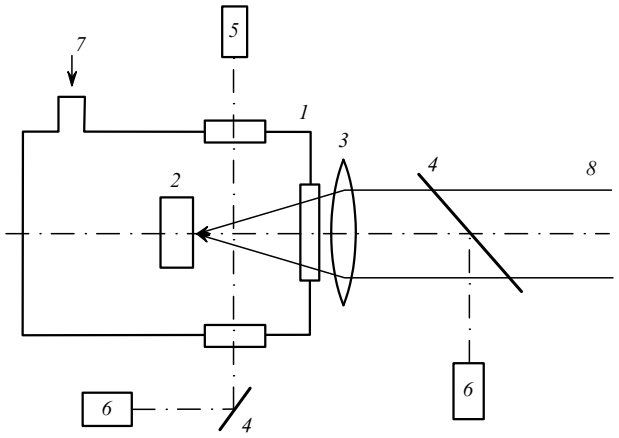

Figure 1. Scheme of the experimental setup: (*1*) chamber; (*2*) target; (*3*) focusing lens; (*4*) deflectors; (*5*) He–Ne laser; (*6*) photomultiplier; (*7*) buffer gas inlet; (*8*) laser beam.

The Nd : glass laser system consisted of a master oscillator and an amplifier. A quasi-continuous regime was obtained by using in the master oscillator an almost concentric cavity, which provided a small modulation depth ($\sim 15\,\%$) of the radiation pulse. Laser radiation was focused on the target with a spherical lens having a focal length of 300 mm to a spot of diameter ~ 1 mm.

We used dielectrics and metal targets and targets made of mixtures of dielectric and metal powders compressed under a pressure up to 150 atm. The finely dispersed phase formed in the laser plume was deposited on a glass substrate for 15 minutes. The optical density of the layer was chosen as a measure of the efficiency of fractal formation. By varying the laser pulse energy and the target position relative to the laser-beam caustic, we could study the efficiency of fractal formation as a function of the size of the irradiated spot and the laser radiation power density.

We also studied the intensity of the laser-plume emission (photoelectronic recording) and its spectrum using a spectral attachment with a diffraction grating from a VFU-1 spectrometer. The spectra were recorded with a CCD array with a time interval of 3 ms. The brightness temperature of the plasma was determined from the ratio of emission intensities of the plume and a standard brightness source at a wavelength of 0.47 μm. The emission of the plume was detected with the help of a FEU-30 photomultiplier and a preset emission wavelength was selected with an interference filter with a transmission bandwidth of 10 nm. As a standard source, a SI8-200U tungsten ribbon filament lamp was used, which was placed during calibration at the target position to eliminate the effect of the geometrical factors.

The size of the plume was determined by photography using various methods, including high-speed photodetection. Laser radiation was directed, as a rule, along the normal to the target surface. When the angle of incidence of the heating radiation flux was larger than its focusing angle, two plumes were observed: a vapour–gas flow propagating along the normal to the surface, and a combustion wave [9] counterpropagating relative to the laser beam. In laser experiments with a similar geometry, the term 'breakdown wave' is normally used [10]. In our case, the laser radiation power densities were insufficient for a breakdown of the buffer gas as well as for sustaining an optical combustion wave in it. The results of test experiments proved that emission of the discharge region at the surface of a molybdenum foil disappeared immediately after the burning of a through hole in the metal. The decisive role in the propagation of a combustion wave obviously belongs to the vapour and the finely dispersed component of the plume.

3. Experimental Results

3.1 Effect of external pressure

The oscillograms of the plume emission presented in Fig. 2 reflect the characteristic changes in the discharge region with increasing the buffer gas pressure p: above a certain threshold value, the emission intensity increases abruptly by almost two orders of magnitude, and an instability is observed during evaporation. Note that in our experiments, the time of formation of the vapour–gas flow is almost independent of the external pressure. Fig. 3 shows the behaviour of the efficiency of fractal formation, emission, and the longitudinal size of the plasma plume upon a change in the buffer gas pressure for a laser plume at the surface of an iron target.

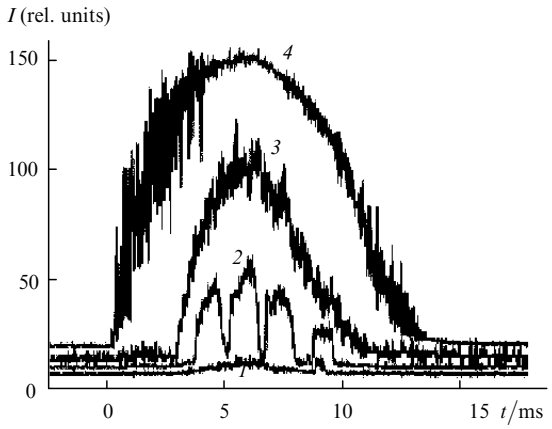

Figure 2. Typical oscillograms of the emission intensity I of the plume under the buffer gas (Ar) pressure $p = 1$ ($p \leqslant p_1$) (curve *1*), 5 ($p \approx p_2$) (curve *2*), and 10 atm ($p > p_3$) (curve *3*), as well as the shape of the laser pulse (curve *4*) for a Ni target.

The efficiency of fractal formation has a distinct maximum at a pressure p that is mainly determined by the material of the target. The emission of the plume increases abruptly at this or a slightly higher pressure p_2. The efficiency decreases with increasing pressure synchronously

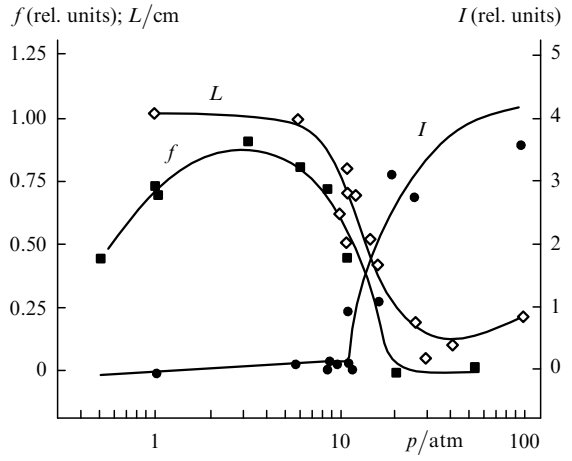

Figure 3. Efficiency f of fractal formation, luminous intensity I, and the longitudinal size L of the plume as functions of the buffer Ar gas pressure p for an iron target.

with a decrease in the length of the emitting region. The emission achieves a maximum when the longitudinal size of the discharge region attains its minimum value equal to its transverse size and, hence, to the diameter of the laser beam waist. The expansion of the plasma is obviously limited not only by the counter-pressure exerted by the buffer gas, but also due to the existence of a certain connectivity either in the cooled layers of the plume or in the plasma itself, which follows from the decisive role of the target material.

Table 1 contains the experimental results obtained during evaporation of various media by laser radiation with a power density of 10^6 W cm^{-2} in argon atmosphere. Note that the buffer gas composition also plays a noticeable role. For example, it was found that during the evaporation of corundum, iron and vanadium, the replacement of argon by helium increases the values of pressure p_1 and p_2 by a factor of about 2. Table 1 gives characteristic pressure values corresponding to the maximum efficiency of fractal formation (p_1), the combustion wave threshold (p_2), and the minimum longitudinal size of the laser plume (p_3), as well as the brightness temperatures describing the emission of the laser-plume plasma for two fixed pressures $p = 1$ and 30 atm.

Table 1. Pressures of the buffer Ar gas corresponding to the maximum efficiency of fractal formation (p_1), the onset of the emission jump (p_2), and the minimum longitudinal size of the plume (p_3), as well as the brightness temperatures T corresponding to the experimental conditions. The errors in determining the temperature and pressure are 15 % and 20 % respectively.

Substance	p_1/atm	p_2/atm	p_3/atm	T/K ($p = 1$ atm)	T/K ($p = 30$ atm)
Al	3	3	8	2500	6400
V	0.5	0.5	–	3400	7650
Fe	4	5	30	2900	7700
Co	4	4	–	2900	7800
Ni	4	4	–	2900	6750
Zn	20	35	–	2700	8100
Nb	1.5	6	36	3800	7100
Mo	0.5	1	–	3500	5900
Sn	1	1.5	–	2500	6700
W	1	1	–	3500	6200
Al_2O_3	9	8	>85	3300	6700
MgO	4	20	20–30	2700	6600
Ce_2O_3	0.1	0.3	20	3100	6400

In the pressure range below p_1, a developed evaporation regime with a characteristic expansion of the erosion laser plasma formed in the vicinity of the target surface is realised. At a certain pressure (p_3 in Table 1), the emission region has the smallest size and is pressed against the target surface (see Fig. 4). Upon a further increase in pressure, the length of the plasma region starts increasing. The emission region acquires a cylindrical shape with well-defined boundaries. Such a behaviour is the result of a change in the plume propagation regime: the expansion of the erosion plasma is replaced by a much brighter luminous combustion in the bulk of the vapour–gas flow containing the finely dispersed phase. The pressure dependence of the emission intensity has a threshold. The critical (threshold) pressure corresponds to pressure p_2 above which the screening of the surface by the discharge plasma increases noticeably, and

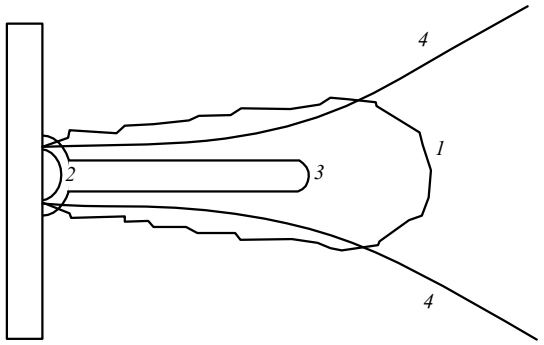

Figure 4. Typical shapes of the plume: (*1*) erosion plume ($p < p_1$); (*2*) plume at the luminous combustion threshold ($p = p_3$); (*3*) light combustion regime ($p > p_3$); and (*4*) laser radiation caustic.

the emissive power of the plume in the direction opposite to the thermal laser radiation becomes considerably higher.

In the pressure range below p_1 in which the laser radiation absorption by the plasma and the plasma emission are relatively weak, the emission spectrum exhibits vibrational bands characteristic of molecules of the evaporated material, e.g., dimers, oxides, etc. We failed to identify the spectral lines of the atoms and ions of the target material and the buffer gas against the background of the vibrational bands. These lines are observed, as a rule, during irradiation of the target in vacuum. For pressures below p_1, the brightness temperature obtained by taking into account the correction to the plasma emissivity (~ 0.1) varies with pressure in accordance with the saturation curve. In the region $p > p_2$, the vibrational bands are broadened noticeably and overlap with increasing pressure. In the light combustion regime, the emission spectrum represents a continuum characterised by a brightness temperature, which depends weakly on the target composition (see Table 1).

An analysis of the microscopic structure of the fractal layers using the images obtained with a scanning electron microscope and presented in Fig. 5 leads to the conclusion that the decrease in the efficiency at high pressures is accompanied by a convolution of fractals, resulting in a

decrease in the fractal dimensionality of structures and an increase in the size of their elementary sites. For pressures below p_1, the fractal structures contain linear fragments of length ~ 2 μm assembled from microscopic particles of size ~ 50 nm, while for pressures above p_1 the microparticle size increases up to ~ 100 nm. In addition, individual solidified drops, and even chains consisting of 10–20 monodispersed spheres, appear in deposited layers (see Fig. 5b).

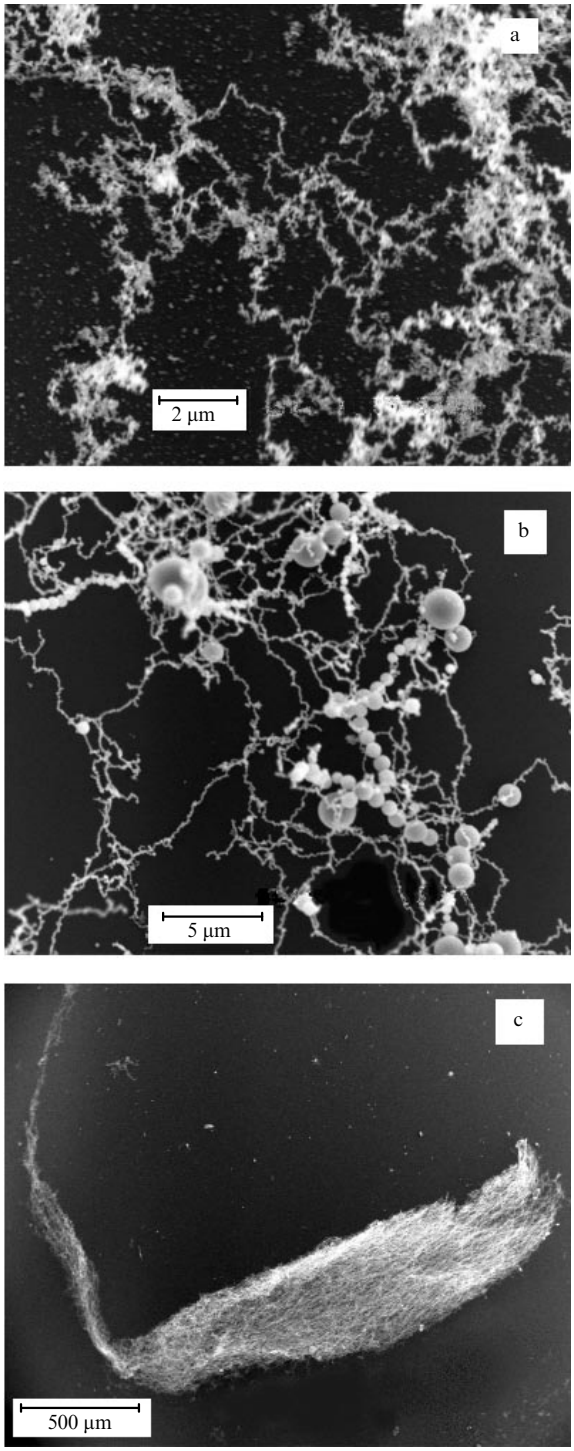

Figure 5. Electron microscope images of fractal layers (a, b) and fractal shell (c) obtained during evaporation of an iron target in Ar atmosphere under a pressure of 0.1 (a) and 12.5 atm (b, c).

The fractal dimensionability was determined from the angular dependence of the intensity of He–Ne laser radiation scattered by fractal layers, and by using the block method [11] for an individual cluster. The fractal dimensionability of the structures shown in Figs 5a and 5b is 1.8 and 1.5, respectively. The thickness of the fractal layer and the size of individual clusters decrease with increasing pressure. Under sufficiently high pressures $p > p_3$, many drops of diameter ~ 1 μm are observed on the cover glass instead of a layer of branching fractals. We can assume that at large pressures and a high temperature of the discharge plasma with confined expansion, the droplets are formed due to compaction of structures and a decrease in the inner surface of a fractal, and is accompanied by the release of the energy stored in it [12].

3.2 Dependences on radiation power density

Fig. 6 shows the dependences of the efficiency of fractal formation and the light sum (integral of the emission intensity of the plume over the pulse duration) on the laser radiation power density q. An iron target was evaporated in the argon atmosphere. Obviously, the threshold power density for fractal formation is that for which the developed evaporation regime appears. In the case of iron, the threshold density is $q_{\text{th}} \sim 0.2 \times 10^6$ W cm^{-2}. For low pressures (< 3 atm), only a layer of fractals is observed on the cover glass for all radiation powers used in the experiments, whereas in the pressure range 4–15 atm, macroscopic fractal structures are observed on the cover glass in addition to the layer of fractals when the power density only slightly ($\sim 30\,\%$) exceeds the threshold value (see Fig. 5c). The macroscopic structure in the form of a wrinkled network shell formed by bound fractal clusters has the following characteristic sizes: $l \sim 1$ cm, and $d \sim 0.1$ cm. The shells that are often split into coarse fragments, are observed immediately after the termination of laser radiation. For higher radiation power densities, such structures are not formed regularly, and are encountered less frequently in Ar than in He. We can assume that the bound shell formed around the plume in the pressure range $p_1 < p < p_3$ drops off as a single entity at low densities of laser radiation power, and is destroyed at high densities.

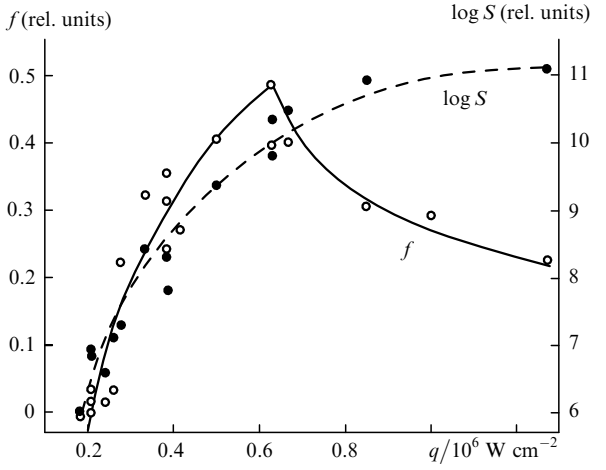

Figure 6. Efficiency f of fractal formation and the logarithm of the light sum S as functions of the laser radiation power density q for an iron target.

The dependence of the light sum on the radiation power density q also indicates the presence of a critical (threshold) power density. According to Fig. 7, the threshold power density for the appearance of a nonlinear growth of the light sum almost coincides with q_{th} for the process of fractal formation. Above the threshold, the dependence of the light sum on the laser power is described by a power function. The exponent of this function is approximately equal to 2 in the erosion plume regime observed under buffer gas pressures $p < p_2$. After a replacement of the combustion regime, the exponent increases up to ~ 10. The light sum depends, in particular, on the delay time of the intense signal relative to the beginning of evaporation. The reason for the delay is the accumulation of the finely dispersed phase in the peripheral regions of the plume.

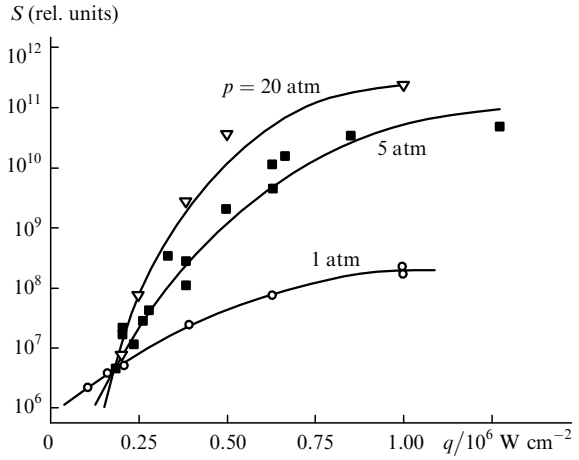

Figure 7. Dependences of the light sum S on the laser radiation power density q for different pressures of the buffer gas obtained for an iron target.

We have found that the delay time depends on the radiation power density and the external pressure – the two parameters determining the density of the evaporated substance in the plasma plume.

4. Discussion

4.1 Fractal shell model

Consider the experimental results on the basis of the model of cavity formation in the bulk of a dust plasma [13]. It is known [7, 13] that an inner cavity containing no microparticles and having well-defined boundaries is formed in a plasma containing charged particles at a rather high concentration along with ions and electrons. The cavity is formed as a result of disbalance between two opposite forces: the electrostatic force $F_{el} = QE$ acting on a particle with charge Q in an electric field E on the one hand, and the forces expelling a microparticle to the periphery of the discharge region on the other hand. For a plasma with a high degree of ionisation, we take into account the force of entrainment of a dust particle during its bombardment by ions [13] and the thermophoretic force [14], which exhibit a quadratic dependence on the particle size in the molecular regime. Because the charge of a particle is proportional to its size, segregation of particles takes place. The particles with a subcritical size are pulled into the cavity by the electrostatic force, while larger particles are expelled from the discharge region.

For a laser-induced plasma, we should also take into account the photoreactive [15] and photophoretic [16] forces directed in most cases along the laser beam. Under the action of these forces, the microparticles return to the target where most of them are evaporated. The low-temperature plasma of a laser plume is a weakly ionised thermal plasma which is characterised by the equality of the temperatures of the electron, ion, and neutral components. In this case, a relatively high temperature gradient is observed. Under these conditions, the microparticles will be expelled to the side boundaries of the torch by the thermophoretic force F_t and by the force F_a of entrainment in the neutral component flow. For particles whose size is smaller than the molecular mean free path in the vapour, these forces are described by expressions [17, 18]:

$$F_t = -2.26\frac{r_0^2 k}{\sigma}\frac{dT}{dx}, \tag{1}$$

$$F_a = \frac{F_s}{B} = -6\pi\eta r_0\frac{u_g - u_p}{B}, \tag{2}$$

where σ is the gas-kinetic cross section for interatomic collisions ($\sigma_{Ar} = 42 \times 10^{-20}$ m^2 and $\sigma_{He} = 15 \times 10^{-20}$ m^2); F_s is the Stokes force, u_g and u_p are the gas and particle velocities; $B = 1 + (\lambda/r_0)[\alpha + \beta\exp(-\gamma r_0/\lambda)]$ is the correction factor introduced for particles of size r_0 smaller than the mean free path λ; α, and β, $\gamma \sim 1$ are constants of the order of unity. The dynamic viscosity η of the buffer gas depends weakly on pressure but exhibits a noticeable dependence on temperature T [19]:

$$\eta = \eta_{T_0}\left(\frac{T}{T_0}\right)\frac{1 + C/T_0}{1 + C/T}, \tag{3}$$

where η_{T_0} is the buffer gas viscosity at room temperature T_0 and C is the Sutherland constant ($C = 142$ for Ar). The viscosity of Ar at the melting points of the substances under study lies in the range $(10 - 20) \times 10^{-5}$ kg m^{-1} s^{-1}. Because the particles are formed in the gas flow in the case under study, the velocities u_g and u_p are almost identical and we can estimate the neutral drag force by assuming that their values differ by less than 10 %. Under these assumptions, we find that, in accordance with expressions (1) and (2), the thermophoretic force is more than double the force of neutral drag, and is equal to $\sim 2 \times 10^2 r_0^2$ N, where $r_0 < 10^{-6}$ m.

As soon as the particle velocity produced by the thermophoretic force becomes higher than the velocity of the vapour – gas flow, a brake force described by the Stokes formula comes into play. Beyond the temperature profile where the thermophoretic force ceases to act, the particles continuing their motion by inertia are decelerated by the stationary buffer gas. Estimates show that the brake force acting on a submicrometer particle is close in order of magnitude to the neutral drag force. As a result, a layer in which coarse particles are accumulated is formed near the boundaries of the discharge region. As their concentration approaches a critical value, the brake force increases nonlinearly because the particles combine to form finite-size clusters (the so-called subcritical clusters). The particle flow stops at a certain distance from the discharge region. The apperance of an infinite-size cluster at the percolation

threshold is accompanied by the formation of a bound structure – a shell embracing the entire plume.

The higher the buffer gas pressure and the density of the vapour – gas phase, the higher the rate of formation of compact clusters and fractal aggregates, and the smaller the distance from the region where the fractal layer stops to the plasma and caustic of laser radiation. After the formation of the shell, a subsequent inflow of the fractal aggregates increases the shell thickness towards the plume axis. The thickness of the shell increases more rapidly at higher radiation power densities. As a result, the layer with the fractal concentration close to the percolation threshold may turn out to be inside the laser radiation caustic. When the shell overlaps the laser beam caustic quite substantially, the inner surface of the shell melts and even evaporates, and the efficiency of fractal formation decreases. Drops are formed on the inner surface of the macrofractal shell.

4.2 Combustion wave within a fractal shell

A fractal shell in the field of laser radiation may significantly alter the breakdown threshold in the inner cavity, as well as the optical characteristics of the discharge. In experiments with dust plasma [7], the formation of a cavity free of dust particles is accompanied by an increase in the electron density and the ionisation rate in the cavity volume. The emission intensity also increases accordingly. At the threshold of cavity formation, an instability appears, which is manifested in emission pulsations similar to those observed in our experiments (see Fig. 2).

The fractal structure of the shell surrounding the laser plume must affect the heat removal from the discharge region [12] on the one hand, and the laser energy supply on the other hand. Because a percolation (fractal) cluster contains 'dead' fibres [20] whose length is more than an order of magnitude larger than their diameter (see Fig. 5), the electric field of the light wave is considerably amplified at the ends of these fibres [21]. Moreover, the permittivity of the medium at the percolation threshold exhibits a divergence [22], and self-action effects for laser radiation should be expected at the boundary of the fractal layer. These effects may include self-focusing of laser radiation, localisation of photons in the fractal structure [23], and amplification of the nonlinear optical response caused by the excitation of dipole moments in fractals near the percolation threshold [24].

5. Conclusions

A plasma produced upon irradiation of condensed media by moderate-power laser pulses at elevated pressures is an effective source of microscopic and macroscopic fractals. Fractals appear during the action of a laser pulse due to the following sequence of processes: (1) vapour condensation accompanied by the formation of compact clusters; (2) expulsion of these clusters by the thermophoretic force to the periphery of the laser plume; (3) their deceleration by the Stokes force and accumulation of clusters in a layer surrounding the discharge plasma; and (4) aggregation into a weakly bound fractal microclusters at low densities of the evaporated material, or into a strongly bound macroscopic fractal structure (shell) above a certain critical density of particles. The behaviour of the laser-plume plasma with a finely dispersed phase is similar in many respects to the behaviour of a dust plasma and is characterised by a threshold-type formation of the inner cavity with distinct boundaries and intense emission.

References

1. Sidorov L.N., Korobov M.V., Zhuravleva L.V. *Mass-spektral'niye termodinamichekie issledovaniya* (Mass-Spectroscopic Thermodynamic Studies) (Moscow: Izd. Moscow State University, 1985).
2. Smirnov B.M. *Usp. Fiz. Nauk*, **164**, 665 (1994).
3. Lushnikov A.A., Nechin A.E., Pakhomov A.V., Smirnov B.M. *Usp. Fiz. Nauk*, **161**, 113 (1991).
4. Kask N.E., Fedorov G.M. *Kvantovaya Elektron.*, **20**, 527 (1993) [*Quantum Electron.*, **23**, 512 (1993)].
5. Kask N.E., Fedorov G.M. *Vestn. Mosk. Univ. Ser 3. Fiz., Astron.*, (6), 25 (1997).
6. Kask N.E., Michurin S.V., Fedorov G.M. *Teplofiz. Vys. Temp.*, **37**, 13 (1999).
7. Samsonov D., Goree J. *Phys. Rev. E*, **59**, 1047 (1999).
8. Samsonov D., Goree J. *J. Vac. Sci. Technol. A*, **17**, 2835 (1999).
9. Bufetov I.A., Prokhorov A.M., Fedorov V.B., Fomin V.K. *Kvantovaya Elektron.*, **8**, 751 (1981) [*Sov. J. Quantum Electron.*, **11**, 453 (1981)].
10. Kovalev A.S., Popov A.M., Rakhimov A.T., Seleznev B.V., Khropov S.M. *Kvantovaya Elektron.*, **12**, 713 (1985) [*Sov. J. Quantum Electron.*, **15**, 468 (1985)].
11. Halsy T., Jensen M., Kadanoff L., Procaccia I., Shraiman B. *Phys. Rev. A*, **33**, 1141 (1986).
12. Smirnov B.M. *Usp. Fiz. Nauk*, **161**, 171 (1991).
13. Morfill G.E., Thomas H.M., et al. *Phys. Rev. Lett.*, **83**, 1598 (1999).
14. Epstein P.S. *Phys. Rev.*, **23**, 710 (1924).
15. Askaryan G.A., Moroz E.M. *Zh. Eksp. Teor. Fiz.*, **43**, 2312 (1961).
16. Kutukov V.B., Shchukin E.R., Yalamov Yu.I. *Zh. Tekh. Fiz.*, **45**, 626 (1975).
17. Rothermel H., Hagl T., Morfill G., Thomas H. *physica/0110045*, v.1, (2001).
18. Stoffels E., Stoffels W.W., Kroesen G.M.W., de Hoog F.J. *Electron. Technol.*, **31**, 255 (1998).
19. Kikoin I.K., (Ed.) *Tablitsy fizicheskikh velichin* (Tables of Physical Quantities) (Moscow: Atomizdat, 1976).
20. Herman H.I., Hong D.C., Stanley H.E. *J. Phys. A*, **17**, L261 (1984).
21. Kovalev A.S., Popov A.M. *Zh. Tekh. Fiz.*, **50**, 333 (1980).
22. Efros A.L., Shklovskii B.I. *Phys. Stat. Sol. b*, **76**, 475 (1976).
23. Maksimenko V.V., Lushnikov A.A. *Pis'ma Zh. Eksp. Teor. Fiz.*, **57**, 204 (1993).
24. Kim W., Safonov V.P., Shalaev V.M., Amstrong R.L. *Phys. Rev. Lett.*, **82**, 4811 (1999).